Introducing Partial Polarimetric Layers into a Curvelet-based Change Detection

Andreas Schmitt, Birgit Wessel
German Aerospace Center (DLR) – German Remote Sensing Data Center, Oberpfaffenhofen, Germany

Abstract

In this article a new change detection approach for polarimetric SAR data is presented. The further development of an already published change detection approach based on Curvelet transform for single polarized SAR images is combined with partial polarimetric layers of a reduced Huynen decomposition. The data used has been acquired by TerraSAR-X in the High Resolution Spotlight mode with two polarization channels: HH and VV (dualpol). The motivation for using polarimetric information is that it helps to interpret changes indicated by the change detection algorithm, so that plant growth or crop on agricultural land as well as water level variations in rivers or even small scale changes in industrial plants like harbors get clearly visible. The Curvelet-based change detection turns again out to be a powerful tool for SAR image handling – image enhancement and change detection – whereas the polarimetric information about the underlying scattering mechanisms delivers astonishing results.

1 Introduction

Both, SAR change detection and SAR polarimetry have been fields of interest during the last decades. While change detection is able to map changes captured in an image pair, it is not easy at all to interpret these changes. In contrast, polarimetry holds much information about the underlying scattering mechanism, but the application of this knowledge is still rudimental. Therefore, the authors intend to exploit synergy effects of both topics by introducing partial polarimetric layers into the Curvelet-based change detection. In the following, the fundamentals of the used SAR techniques are outlined, before this new approach is applied exemplarily to one SAR test site. The interpretation of the mapped changes and the conclusion complete this article.

2 Theoretical background

In this chapter the previous works concerning Curvelets and SAR polarimetry are roughly summarized and the transition of the standard techniques to partial polarimetric change detection is explained.

2.1 Curvelets

The Curvelet transform has originally been developed for the compression of optical images. An image containing discontinuities along curves, i.e. edges can be described by a minimal number of coefficients using the Curvelet representation [1]. Many investigations were necessary to assimilate the Curvelets defined in a continuous space to the discrete space and to accelerate the computation also for larger images or for higher dimensions [2]. Several implementations of the Curvelet transform as well as some demo versions are available on the Curvelet homepage [3]. The advantage of Curvelets over other alternative image descriptions, e.g. like wavelets, particularly in the context of SAR images is the capability to adapt structures not only to several scales and positions but also to different orientations. So, we call it a structure-based image description [9].

2.2 Curvelet-based Change Detection

In the context of surveying man-made objects, e.g. urban areas, one is interested in mapping changes in the structures apparent in a SAR image instead of changes concerning single points or large regions. If two SAR images are compared pixel by pixel, many changes are indicated that are derived exclusively from the high noise level. One possibility is to smooth the image using large windows to suppress point-like noise and to get laminar changes. As structures consequently get lost, this approach is not suitable for fine-structured areas. For those applications our Curvelet-based change detection method was designed, where the differentiation is done in the Curvelet coefficient domain instead of the spatial domain [8]. After the Curvelet transform a huge amount of complex coefficients describes the input images by means of linear structures that differ in position, scale

and orientation [9]. These coefficients of both images are differentiated and weighted by a special function that suppresses low coefficients and amplifies stronger coefficients in order to remove clutter and to enhance structures. The threshold in-between is determined by an iterative process that discriminates existent structures from background noise. This algorithm removes strong coefficients – associated with structures – until the remaining ones possess a normal distribution. The inverse transform of the weighted coefficients produces a nearly noise-free difference image including only the changes concerning underlying linear structures.

2.3 Partial polarimetric decomposition

SAR polarimetry has been a research topic for many years. Many scientists designed new decompositions for special applications. An overview to actual standard decompositions is given in some reviews [4],[5]. The problem with all of the decompositions is the availability of adequate data. Nowadays, most SAR satellites are able to acquire data in more than one polarization direction, but not all satellites deliver full polarimetric data in all acquisition modes. Hence, the user has to balance reasons for a polarimetric evaluation on the one hand or a much better resolution on the other hand. In this article we agreed to avail TerraSAR-X High Resolution Spotlight data with only two polarizations (HH&VV). These images share a pixel-spacing on ground of 1 m in the spatially enhanced *Enhanced Ellipsoid Corrected* product type. The Single Look Complex data has been combined according to the Huynen decomposition [6]. This decomposition has been chosen, because it provides three independent polarimetric layers that can be decomposed out of HH and VV polarization (Eq. 1) without the cross polarized layer.

$$2A_0 = \tfrac{1}{4}\left\langle \left| HH + VV \right|^2 \right\rangle \qquad (1)$$

$$B_0 - B_\varphi = \tfrac{1}{4}\left\langle \left| HH - VV \right|^2 \right\rangle$$

$$C_\varphi + iD_\varphi = \tfrac{1}{4}\left\langle \left| HH \right|^2 - \left| VV \right|^2 + 2i\,\mathrm{Im}(HH * VV) \right\rangle$$

The component A_0 can be denoted as total scattered power from the regular, smooth, convex parts of a scatterer, whereas $B_0 - B_\varphi$ represents the total symmetric depolarized power. The other two parameters describe the depolarizing components of symmetric targets: C_φ is the generator of target global shape (Linear) and D_φ of target local shape (Curvature) [7]. The other components of the coherence matrix are omitted here. This "reduced" Huynen decomposition is then color-coded as given in Eq. 2. After the essential averaging (3x3 pixel window), the decomposition layers, still in slant range geometry, are geocoded using DLR's routine for the generation of Enhanced Ellipsoid Corrected products.

$$R: \quad B_0 - B_\varphi \qquad (2)$$

$$G: \quad \frac{\left\langle C_\varphi \right\rangle^2 + \left\langle D_\varphi \right\rangle^2}{A_0 + B_0}$$

$$B: \quad 2A_0$$

3 Sample applications

Now the algorithms described in the preceding chapter are applied to real data sets. The images have been acquired by TerraSAR-X in the High Resolution Spotlight mode with dual polarization (HH/VV) over the cities of Mannheim/Ludwigshafen (Germany) in repeat-pass geometry. The first image dates from, 21.09.2008, the second one from 02.10.2008.

3.1 Image Enhancement

Fig. 1a illustrates the first SAR image in the reduced Huynen decomposition described above (Eq. 2). This subset shows the harbor region: the river Rhine and several harbor basins. The dark regions are smooth water surfaces, where the incident electromagnetic waves are reflected away from the sensor. The blue color marks areas with mainly surface scattering, e.g. sand, where the surface is slightly rougher than the water surface but the undulation is still smaller than the wavelength of TerraSAR-X. The red points and lines respectively refer to diplane scattering, that can be found where two planes are perpendicular to each other and oriented nearly parallel to the flight direction. The green points demonstrate a strong depolarizing component of symmetric scatterers (cf. 2.3). Obviously this scattering type can be found at the edges of really strong scatterers, which appear in white because their backscattering is high in all channels. Unfortunately, this image is still very noisy. If the noise

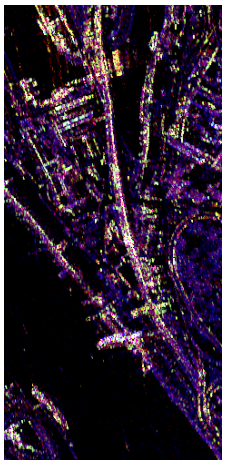

Figure 1a: Reduced Huynen decomposition after geocoding step

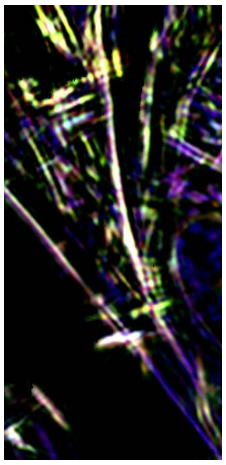

Figure 1b: Enhanced image of Fig. 1a using the Curvelet approach

level is reduced by summing up over larger regions the structures would get lost. So, we applied the Curvelet approach for image enhancement separately on each layer, see Fig. 1b. The image has been smoothened without destroying the structures. The structures apparent have even been intensified. Single pixels of the same scattering type have either been removed or added to larger agglomerates. It is remarkable that the green structures are most amplified in comparison to the blue and red channel. As the green channel shows high values near strong backscatterers, that are mostly man-made and therefore possess a clear geometry, this channel contains also more small scale structures than e.g. the blue channel, where mainly surface scattering is present over large areas (see also Fig. 2). For image interpretation this Curvelet-based enhancement is really helpful removing noise and amplifying structures one is interested in, when looking at urban areas (cf. Fig. 1a&b).

3.2 Change Detection

Then, we have a look on the differences in the single polarimetric channels of the reduced Huynen decomposition calculated by the Curvelet-based change detection. Fig. 2 contains the difference in the "surface scattering" channel. Green structures indicate an increase of surface scattering from the first acquisition to the second, red areas mark a decrease in surface scattering. Large areas on the top and on the right as well as small scale changes in the middle of the image can be perceived. Three red stripes, two on the bottom left and one on the right of the image are remarkable. Along the rivers and basins some green stripes appear that vary in their thickness. The "diplane scattering" channel is depicted in Fig. 3. Again large areas that brightened up are obvious. But in contrast to the preceding layer, the geometry of the regions on the top of the image is different. The fine red and green structures in the middle of the image are similar, on the top left and in the middle right some new red and green structures appear. Along the river no changes are visible in the diplane layer. The third layer, the depolarizing component of symmetric targets, is shown in Fig. 4. Only one large area change remains. The small scale changes in the harbor region (middle of the image) are still existent, but many others – mainly on the left bank of the river – are added. Although these changes are all fine structured they agglomerate to larger regions, where red and green structures are lying next to each other. It is very interesting that these changes also appear in regions, where no changes were mapped in the other two channels and the original images show very high amplitudes. This could be a hint that the "depolarization" channel is much more sensitive towards slight changes happening to strong scatterers.

In summary we can say that the percentage of large scale changes is decreasing from layer one ("surface") to layer three ("depolarization") while the percentage of fine structured changes is obviously increasing. This fact supports the theory that changes show up differently in the different channels and that the combination of the three channels can deliver the basis for a characterization and an interpretation of the changes mapped by the help of this approach.

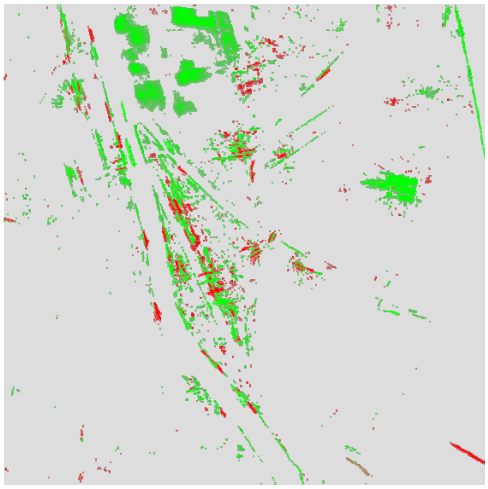

Figure 2: Difference image channel B

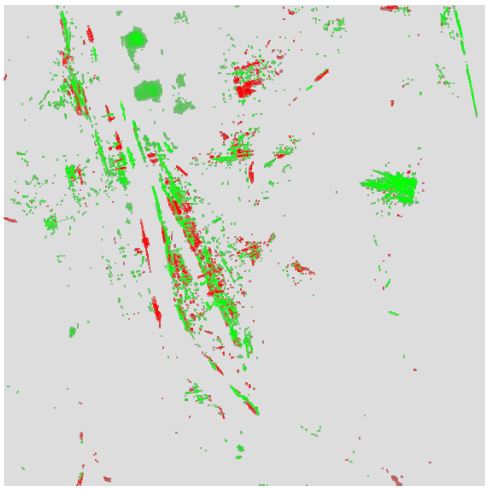

Figure 3: Difference image channel R

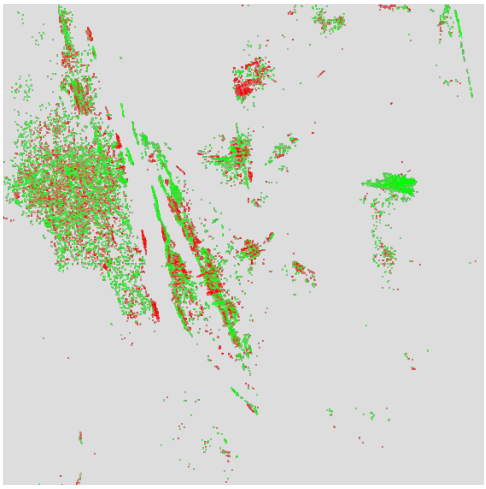

Figure 4: Difference image channel G

3.3 Change Interpretation

If the difference images depicted in Fig. 2-4 are transformed to grey value images and than combined in a RGB image – according to Eq. (2) – the changes appear in different colors depending on the contribution of the three layers (see Fig. 5). To simplify the interpretation, only positive changes are depicted, but negative changes can be displayed in a uniform manner.

Blue indicates an increase in the surface scattering component, the red color stands for an increase in the diplane scattering power. Starting on the top of the image there are larger regions in blue and in red over agricultural land. These changes can surely be referred to the crop, where plants are removed and the influence of the bare soil causes an increase of surface scattering or the dry remains of the grain (e.g.) cause a higher diplane scattering. Along the river a slight blue line is visible. This line is thicker outside the urban area and disappears completely in the harbor region. So, this change could be influenced by the different fortifications: walls in the harbor and sand banks outside the city. As smooth water surfaces show nearly no backscatter, these changes have to be caused by the banks: they were enlarged, because of a sinking water level. This assumption is proven by a look on the water level dates for Speyer (31 km upstream), where the gauge of 4 m is registered for the first acquisition and only 3 m for the second one [10]. White areas map changes apparent in all three channels, mostly present on the fairground of Mannheim, where pavilions are erected for the “Oktobermess” festival in-between the two image acquisitions. The behavior of the green “depolarizing” layer is most interesting. High values are restricted to purely industrial areas with a high density of strong single backscatterers that have probably been slightly moved since the last image acquisition. So, these regions stick out of all other built-up areas.

Figure 5: Color composition of Fig. 2, 3 and 4

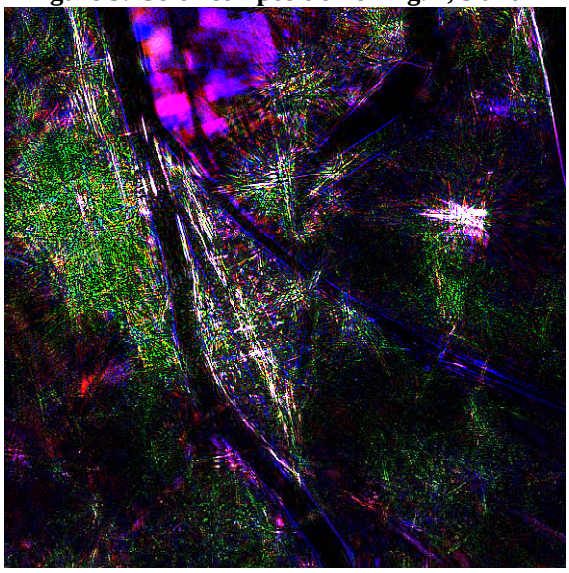

4 Conclusion

In this article we presented an extension of the Curvelet-based change detection approach. It has been applied to TerraSAR-X dual polarized data in a reduced version of Huynen’s decomposition. While the interpretation of the changes mapped by the comparison of single polarized images is always very difficult, the changes now can clearly be attached to special scattering effects using polarimetric SAR data. As this first attempt was surprisingly successful, we will concentrate on the inclusion of further polarimetric channels into the change detection approach in future.

References

[1] Candès, E. J.; Donoho, D. L.: *Curvelets – a surprisingly effective nonadaptive representation for objects with edges*. Innovations in Applied Mathematics, pp. 105-120, Vanderbilt University Press, Nashville (TN-USA), 1999

[2] Candès, E. J.; Demanet, L.; Donoho, D. L.; Ying, L.: *Fast Discrete Curvelet Transforms.* Multiscale Modeling and Simulation, Vol. 5, No. 3, pp 861-899, Philadelphia (PA-USA), 2005

[3] Demanet, L.: *curvelet.org*. Curvelet homepage, http://www.curvelet.org, last access 04.02.2010

[4] Cloude, S. R.; Pottier, E.: *A Review of Target Decomposition in Radar Polarimetry.* IEEE Transactions on Geoscience and Remote Sensing, Vol. 34, No. 2, pp. 498-518, 1996

[5] Touzi, R.; Boerner, W. M.; Lee, J. S.; Lueneburg, E.: *A Review of polarimetry in the context of synthetic aperture radar: concepts and information extraction*. IEEE Transactions on Geoscience and Remote Sensing, vol. 30, No. 3, pp. 380-407, 2004

[6] Unal, C. M. H.; Lighart, L. P.: *Decomposition theorems applied to random and stationary radar targets.* PIER Progress in Electromagnetic Research, Vol. 18, pp. 45-66, 1998

[7] Ferro-Famil, L.: *Polarimetric Decompositions*. Polarimetry Tutorial of European Space Agency, http://www.earth.esa.int/polsarpro/tutorial.html, last access 23.10.2009

[8] Schmitt, A.; Wessel, B.; Roth, A.: *Curvelet Approach for man-made Objects from SAR Images*. Proceedings of IGARSS 2009, Cape Town (South Africa), 2009

[9] Schmitt, A.; Wessel, B.; Roth, A.: *Curvelet Approach for SAR Image Denoising, Structure Enhancement, and Change Detection*. Proceedings of CMRT 2009, Paris (France), 2009

[10] http://wetteronline.de, Pegel Speyer/Rhein, denoted data source: Bundesanstalt für Gewässerkunde, last access 23.10.2009